Journal of Molecular Structure 1265 (2022) 133296

Contents lists available at ScienceDirect

Journal of Molecular Structure

journal homepage: www.elsevier.com/locate/molstr

Synthesis, crystal structure and catalytic activity of the new hybrid phosphate $(C_4H_{12}N_2)[Co(H_2O)_6](HPO_4)_2$

Safaa Hidaoui[a], Najlaa Hamdi[a], Mohamed Akouibaa[a], Rim Benali-Cherif[b], Eigner Vaclav[c], Michal Dusek[c], Mohammed Lachkar[a], Brahim El Bali[d,*]

[a] Engineering Laboratory of Organometallic, Molecular Materials, and Environment, Faculty of Sciences, University Sidi Mohamed Ben Abdellah, 30000 Fez, Morocco
[b] Laboratoire des Structures, Propriétés et Interactions Interatomiques, Université Abbes Laghrour Khenchela, 40000 Khenchela, Algeria
[c] Institute of Physics AS CR, v.v.i., Na Slovance 2, 182 21 Prague 8, Czech Republic
[d] Independent Scientist, Oujda, Morocco

ARTICLE INFO

Article history:
Received 22 December 2021
Revised 13 April 2022
Accepted 11 May 2022
Available online 13 May 2022

Keywords:
Hybrid phosphate
Crystal structure
Hirshfeld surface
Catalysis

ABSTRACT

A new hybrid phosphate $(C_4H_{12}N_2)[Co(H_2O)_6](HPO_4)_2$ has been synthesized using wet chemistry. The compound crystallizes in the monoclinic system, space group $P2_1/c$, the cell parameters (Å, °): [a = 6.2959(2), b = 9.5613(3), c = 12.7942(4), β = 92.718(3), V = 769.31(4) Å^3 and Z = 2]. Its crystal packing is made of isolated $[Co(H_2O)_6]$ octahedra, regular $[PO_3(OH)]$ tetrahedra and diprotonated piperazine $[C_4H_{12}N_2]^{2+}$, which interact through hydrogen bonds. The Hirshfeld surface and 2D fingerprint plots have been performed to explore the features of the crystal cohesion. The main contributions are provided by O···H/H···O contacts. The Fourier Transform Infrared spectroscopy shows the expected bands of piperazine and phosphate groups. The catalytic efficiency was tested with the reduction reaction of the three nitrophenol isomers (paranitrophenol 4-NP, metanitrophenol 3-NP and orthonitrophenol 2-NP), and was applied as an oxidant for the degradation of methylene blue in aqueous solutions.

1. Introduction

Hybrid inorganic-organic materials are of great interest owing to their rich structural chemistry and their wide applications in many fields like absorption, catalysis, ion exchange and separation [1–7]. They are conveniently classified in two main classes, depending on the magnitude of interactions between the phases [8]. Class I is devoted to materials that imply weak interactions such as Van der Waals and hydrogen bonds, while class II contains materials exhibiting strong covalent or iono-covalent bonds. Within class I, derivatives from orthophosphoric acid (H_3PO_4) are often associated with functionalized organic molecules (amides or amines) to provide organic-inorganic materials with potentially forceful hydrogen-bonding interactions. Among these materials, hybrid cobalt phosphates such as $[C_4N_{11}H_2][Co_2(PO_2)(H_2PO_4)_2]$ and $[C_4N_2H_{12}][Co(HPO_4)_2]$ have been found to be an important group that exhibits various dimensionalities and generates new functionalities [9]. Generally, hybrid assemblies are synthesized either via hydrothermal method or through wet chemistry process, employing organic molecules as bridging ligands that bond via nitrogen to the metal centers or as templates of metal phosphates by hydrogen bonding interactions [10–12]. Hence, such directing agents play a key role in tuning the structures of the obtained materials by means of size, polarity, charge and shape. Furthermore, the self-assembly of these compounds is mainly governed by weak energy bonding that exhibits a supramolecular open framework, which can be used as a trapping matrix due to their porous structures within which molecules or ions can be trapped and stored, leading consequently to a large variety of new topologies [13,14]. In this context, we report in the present study on the chemical preparation, crystallographic description coupled with Hirshfeld surface analysis, spectroscopic characterization and thermal behavior of a novel cobalt phosphate $(C_4H_{12}N_2)[Co(H_2O)_6](HPO_4)_2$. As a matter of application, the new hybrid phosphate was tested as a catalyst for the oxidation and degradation of methylene blue dye and as a catalyst in the reducing of three nitrophenol isomers (i.e.: paranitrophenol 4-NP, metanitrophenol 3-NP and orthonitrophenol 2-NP) to their corresponding aminophenol isomers.

* Corresponding author.
E-mail address: b_elbali@yahoo.com (B.E. Bali).

https://doi.org/10.1016/j.molstruc.2022.133296
0022-2860/

Table 1
Experimental data collections details for $(C_4H_{12}N_2)[Co(H_2O)_6](HPO_4)_2$.

Crystal data	$(C_4H_{12}N_2)[Co(H_2O)_6](HPO_4)_2$
Chemical formula	447.1; 466
Mr(g/mol); F(000)	Monoclinic ($P2_1/c$)
Crystal system (S.G.)	6.2959(2), 9.5613(3), 12.7942(4); 92.718
a, b, c (Å); β (°)	769.31(4); 2
V(Å^3); Z	$0.70 \times 0.49 \times 0.36$; 1.4
Crystal size (mm); m(mm^{-1})	
Data collection	Xcalibur, AtlasS2, Gemini ultra
Diffractometer	Absorption correction: analytical
Absorption correction	CrysAlis PRO 1.171.38.43 (Rigaku Oxford CrysAlis Diffraction, 2015)
T_{min}, T_{max}	0.536, 0.684
No. of measured, independent and observed [I > 3σ(I)] reflections	13314, 2035, 1867
R_{int}	0.026
Refinement	
R[F^2 >3σ(F^2)], wR(F^2), S	0.022, 0.078, 1.44
No. of reflections	2035
No. of parameters	135
No. of restraints	9
H-atom treatment	H atoms treated by a mixture of independent and constrained refinement
$\Delta\rho$max, $\Delta\rho$min (e.Å^{-3})	0.36, -0.24

JANA2006 does not refine the weighting scheme. Therefore, the goodness of fit is usually fairly above 1, especially for well-exposed data containing information about bonding electrons.

2. Experimental

2.1. Crystal synthesis

Crystals of $(C_4H_{12}N_2)[Co(H_2O)_6](HPO_4)_2$ were synthesized using a wet chemistry route. A mixture of 10 mmol (0.6 mL) of H_3PO_4 acid (85%) (Prolabo) and 3.36 mmol (0.40 g) of $CoCO_3$ (Prolabo) was dissolved at 80°C in 20 mL of distilled water. After 1h of continuous stirring, a quantity of piperazine (1M) was added to the pink solution, final pH = 5. The mixture were left for 4 weeks at room temperature, after which pink crystals were collected and washed with the water-ethanol mixture (80:20), and then dried in air.

22. Crystal structure determination

Crystal structure determination by X-ray diffraction was performed on Oxford diffraction CCD diffractometer Gemini with graphite-monochromated MoKα ($\lambda = 0.7173$ Å) radiation at 120 K, registered with an Atlas S2 CCD area detector. Data were processed with the program Crysalis PRO [15]. The phase problem was solved by charge flipping methods using the program Superflip [16], and the structure was refined with Jana2006 [17]. The structural graphics were generated with the program DIAMOND [18]. Data collection and refinement details of $(C_4H_{12}N_2)[Co(H_2O)_6](HPO_4)_2$ are reported in Table 1. The atomic coordinates are reported in Table 2, the basic geometrical data in Table 3, hydrogen bonds in Table 4. All hydrogen atoms visible in difference Fourier maps, but according to common practice the hydrogen atoms attached to carbon were kept in an ideal position, while hydrogen atoms attached to nitrogen and oxygen were refined with restrained bond lengths. All non-hydrogen atoms were refined anisotropically, while for hydrogen atoms, U_{iso} value was fixed at $1.2U_{eq}$ of their parent atoms. Supplementary crystallographic data might be found in the deposited CIF at CCDC, depositing number 2107736. These data can be obtained free of charge from The Cambridge Crystallographic Data Centre via www.ccdc.cam.ac.uk/structures.

2.3. Hirshfeld surface calculations

Analysis of intermolecular interactions using the Hirshfeld surface was undertaken to gain a better understanding of the three-dimensional crystal packing of $(C_4H_{12}N_2)[Co(H_2O)_6](HPO_4)_2$. Hir-

Table 2
Fractional atomic coordinates and isotropic or equivalent isotropic displacement parameters (Å^2).

	x	*y*	*z*	U_{iso}*/U_{eq}
Co1	0	0	0	0.00642 (10)
P1	0.58121 (5)	0.74589 (3)	0.23262 (3)	0.00755 (11)
O1w	0.08137 (15)	-0.17810 (10)	0.08868 (7)	0.0096 (3)
O2w	-0.09671 (15)	0.10228 (11)	0.13314 (8)	0.0129 (3)
O3w	0.29619 (15)	0.09380 (11)	0.02362 (8)	0.0115 (3)
O1	0.48919 (15)	0.76862 (10)	0.12204 (7)	0.0109 (3)
O2	0.48868 (15)	0.61746 (10)	0.28571 (7)	0.0099 (3)
O3	0.51263 (19)	0.87353 (11)	0.30352 (8)	0.0183 (3)
O4	0.82322 (16)	0.74255 (12)	0.23886 (9)	0.0178 (3)
N1	0.0943 (2)	0.38440 (13)	0.05453 (11)	0.0192 (4)
C1	-0.0885 (3)	0.45955 (18)	0.09623 (14)	0.0294 (5)
C2	-0.2227 (3)	0.52168 (17)	0.00865 (18)	0.0274 (6)
H1c1	-0.172429	0.395621	0.134823	0.0352*
H2c1	-0.03763	0.532539	0.142472	0.0352*
H1c2	-0.337508	0.573449	0.036747	0.0328*
H2c2	-0.281453	0.448218	-0.034926	0.0328*
H1o1w	0.2073 (8)	-0.1926 (18)	0.1041 (13)	0.0115*
H2o1w	0.012 (2)	-0.1925 (19)	0.1403 (8)	0.0115*
H1o2w	-0.012 (2)	0.1435 (16)	0.1728 (11)	0.0155*
H2o2w	-0.2127 (14)	0.1084 (19)	0.1594 (13)	0.0155*
H1o3w	0.360 (3)	0.1330 (18)	-0.0224 (10)	0.022*
H1n1	0.162 (3)	0.3563 (19)	0.1106 (9)	0.023*
H2n1	0.046 (3)	0.3132 (13)	0.0197 (13)	0.023*
H2o3w	0.367 (2)	0.0879 (19)	0.0788 (8)	0.0138*
H1o3	0.500 (5)	0.9458 (16)	0.269 (2)	0.061 (8)*

Table 3
Bond distances (Å) for $(C_4H_{12}N_2)[Co(H_2O)_6](HPO_4)_2$.

Co1—O1w	2.0963 (10)	O3w—H1o3w	0.820 (15)
Co1—O1w^{i}	2.0963 (10)	O3w—H2o3w	0.820 (11)
Co1—O2w	2.0801 (10)	O3—H1o3	0.820 (19)
Co1—O2w^{i}	2.0801 (10)	N1—C1	1.478 (2)
Co1—O3w	2.0784 (10)	N1—C2^{ii}	1.475 (2)
Co1—O3w^{i}	2.0784 (10)	N1—H1n1	0.860 (13)
P1—O1	1.5188 (10)	N1—H2n1	0.860 (14)
P1—O2	1.5317 (10)	C1—C2	1.494 (3)
P1—O4	1.5223 (10)	C1—H1c1	0.96
O1w—H1o1w	0.820 (6)	C1—H2c1	0.96
O1w—H2o1w	0.820 (12)	C2—H1c2	0.96
O2w—H1o2w	0.820 (14)	C2—H2c2	0.96
O2w—H2o2w	0.820 (11)		

Table 4
Hydrogen-bond geometry (Å, °) for $(C_4H_{12}N_2)[Co(H_2O)_6](HPO_4)_2$.

D—H···*A*	*D*—H	H···*A*	*D*···*A*	*D*—H···*A*
C1—H1*c*1···O3^{iii}	0.96	2.33	3.127 (2)	140
C2—H1*c*2···O1^{iv}	0.96	2.44	3.350 (2)	157
O1*w*—H1*o*1*w*···O1^{v}	0.820 (6)	1.817 (6)	2.6326 (13)	173.1 (17)
O1*w*—H2*o*1*w*···O4^{vi}	0.820 (12)	1.880 (14)	2.6843 (15)	166.6 (15)
O2*w*—H1*o*2*w*···O4^{vii}	0.820 (14)	1.860 (14)	2.6792 (14)	178.1 (15)
O2*w*—H2*o*2*w*···O2^{iii}	0.820 (11)	1.907 (11)	2.7262 (14)	177.0 (16)
O3*w*—H1*o*3*w*···O1^{viii}	0.820 (15)	1.877 (16)	2.6960 (14)	176.6 (16)
N1—H1*n*1···O3^{vii}	0.860 (13)	2.283 (16)	3.0012 (18)	141.0 (15)
N1—H1*n*1···O4^{vii}	0.860 (13)	2.210 (13)	2.9944 (17)	151.5 (16)
N1—H2*n*1···O1*w*^{i}	0.860 (14)	2.033 (15)	2.8774 (16)	166.9 (14)
O3*w*—H2*o*3*w*···O2^{vii}	0.820 (11)	1.938 (11)	2.7428 (13)	166.7 (17)
O3—H1*o*3···O2^{ix}	0.820 (19)	1.789 (18)	2.5966 (14)	168 (3)

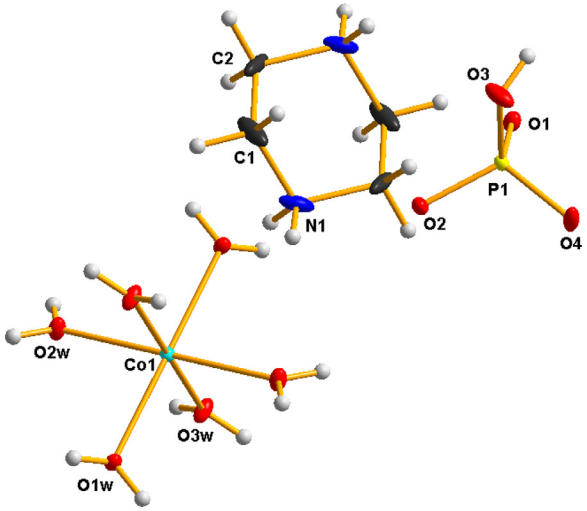

Fig. 1. Organic molecule and metal coordination in the crystal structure of 1, ellipsoids drawn at 50%.

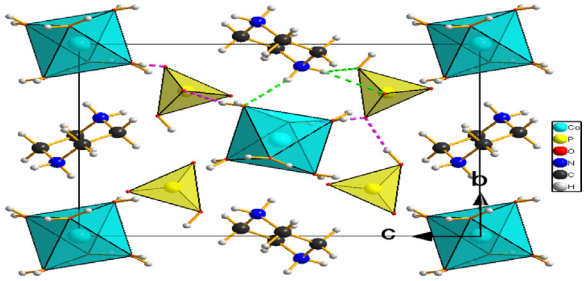

Fig. 2. Projection along [100] of 1, H-Bonds as dashed lines, highlighting the cavities hosting the organics inside the inorganic framework.

shfeld surface (HS) analysis [19] and 2D fingerprint plots [20] were drawn by Crystal Explorer software [21] using experimental structure input file (CIF). This analysis method is employed to study all types of intermolecular forces and non-covalent interactions present in the crystal structure. The d_{norm} normalised contact distance is defined by internal d_i and external d_e distances and the Van der Waals (VdW) radii of the atoms, as follows:

$$d_{norm} = \frac{d_i - r_i^{vdW}}{r_i^{vdW}} + \frac{d_e - r_e^{vdW}}{r_e^{vdW}}$$

in which d_e and d_i represent the distances from the nearest nuclei to the external and internal surfaces, respectively, define the Hirshfeld map with specific coloured contours. The bright red areas on the molecule represent the strong and short contacts, white regions show Van der Waals separation, and blue regions exhibit the closer contacts. The related fingerprint plots were drawn to quantify the percentage contributions of various intermolecular contacts present.

2.4. Infrared spectroscopy

The infrared spectrum of the compound was recorded on a VERTEX 70 FTIR Spectrometer in the range 4000-400 cm^{-1} using the ATR technique with a resolution of 4 cm^{-1}.

2.5. Thermal gravimetric analysis

The thermal stability of the sample was carried out in an air atmosphere using the alumina capsules in a TA60 SHIMADZU thermal analyser simultaneous TGA/DTA. The sample was linearly heated ($T = T_0 +$ b.t) from ambient to 600°C at a rate of 20°C/min.

2.6. Catalytic activity test

2.6.1. Removal of methylene blue

The catalytic achievement of cobalt hybrid phosphate was tested in the oxidation and degradation of methylene blue dye by following an experimental protocol as defined previously in the literature [22]. 45 mL of methylene blue 6 ppm and 5 mL of H_2O_2 30% were mixed into an aqueous solution under continuous stirring at 20°C. The miscellaneous was dark-blue, with an absorption peak located at 665 nm. $(C_4H_{12}N_2)[Co(H_2O)_6](HPO_4)_2$ (0.1 g) was then added to the solution under stirring. The reaction was followed by an ultraviolet-visible (UV-Vis) spectrophotometer. The UV-vis absorption could detect the oxidation of methylene blue; at the same time, we observed that the color of the methylene blue gradually became colorless from dark blue after 240 min, indicating that methylene blue was gradually oxidized.

2.6.2. Nitrophenol reduction test

The hybrid phosphate $(C_4H_{12}N_2)[Co(H_2O)_6](HPO_4)_2$ was tested as a catalyst in the reduction of the three nitrophenol isomers 4-NP, 3-NP, and 2-NP to their corresponding aminophenol isomers. In a typical experiment, 40 mL of a sodium tetrahydroborate $NaBH_4$ solution (8×10^{-4} M) was added under continuous stirring to 40 mL of a para-nitrophenol solution at 4×10^{-4} M. Then, an intense yellow color appeared because of the formation of a para-nitrophenolate anion in the solution, and an absorption peak appears at 401 nm (4-NP), 393 nm (3-NP), and 415 nm (2-NP). The hybrid phosphate Cobalt (0.1 g) is then added to the mixture while stirring. The yellow color of the solution disappears gradually due to the action of the catalyst. The reaction was followed via UV-visible spectrophotometry measurements.

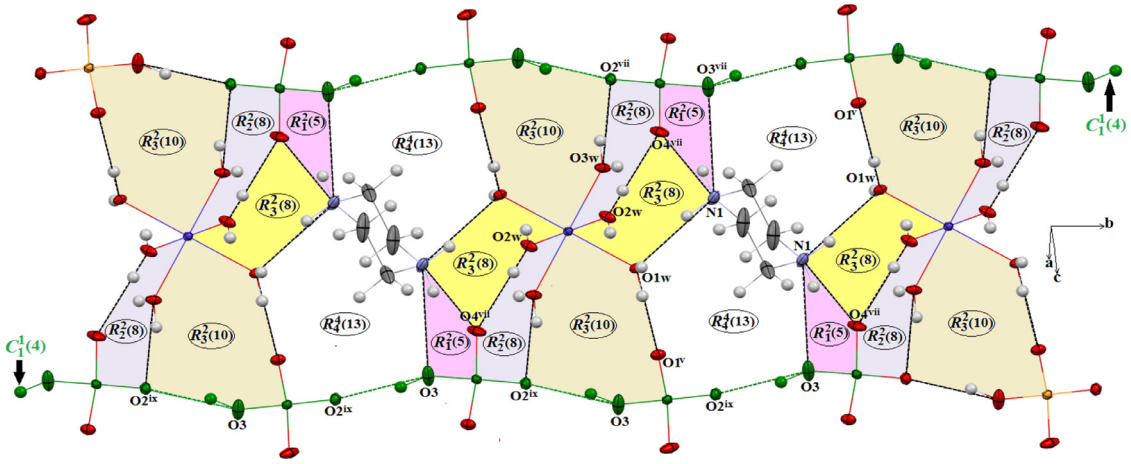

Fig. 3. Part of packing diagram of 1 illustrating the formation of (13), (10), (8), (8) and (5) ring motifs and (4) infinite chain. Dashed lines indicate N—H···O and O—H···O hydrogen bonds.

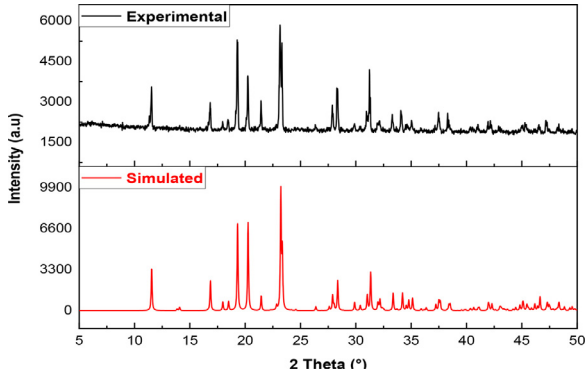

Fig. 4. Simulated and experimental powder X-ray diffraction patterns of 1.

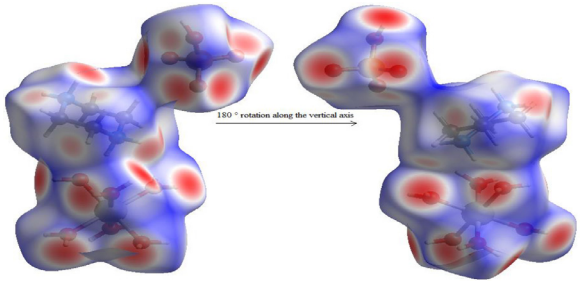

Fig. 5. Two different views of HS mapped with d_{norm} of $(C_4H_{12}N_2)[Co(H_2O)_6](HPO_4)_2$.

3. Results and discussion

3.1. Crystal structural description

The hybrid phosphate $(C_4H_{12}N_2)[Co(H_2O)_6](HPO_4)_2$ (1) crystallises in the monoclinic system ($P2_1/c$). The asymmetric unit contains 12 non-hydrogen atoms, with Co^{2+} located in the Wyckoff site 2a. Its crystal structure consists of isolated Co^{2+} coordinated by six water molecules $[Co(H_2O)_6]^{2+}$, hydrogenphosphate anions $[HPO_4]^{2-}$, and diprotonated piperazine $[C_4H_{12}N_2]^{2+}$ (referred to as $[H_2pip]^{2+}$), which acts as counter-ion entity compensating the negative charge of the inorganic framework (Fig. 1). The synthesized compound 1 belongs to the Class I of hybrid materials where the isolated moieties interact through a network of hydrogen bonds, leading to a supramolecular assembly (Fig. 2).

The piperazine ring adopts the chair conformation with protonation of its nitrogen atoms. The C–C(N) distances range from 1.475(2) to 1.478(2) Å, whilst the C–C–N and C–N–C angles vary between 110.18(15)° and 110.99(12)° (Table 3). These values are close to those found in other materials containing such molecule [23,24]. Co^{2+} lies on the inversion center (0, 0, 0) in a nearly regular octahedron made of six water molecules. The octahedroń bond length distortion value of 6.1347×10^{-9}, according to the formula $\Delta oct = 1/6\times\Sigma[(di\text{-}dm)/dm]^2$ [25,26], is very low compared to 4.532×10^{-3} reported in $[Co(H_2PO_2)(C_{12}N_4H_{16})]Cl_2$ [27]. Within the Co octahedron, Co-O_W distances vary from 2.0784 to 2.0963(10) Å with a mean distance of 2.0849 Å (Table 3), which can be compared to the values reported in $(NH_4)[Co(H2O)_6]_3(HPO_3)_4$ (2.093(2) Å) [28] or 2.092 Å in $(C_6H_{16}N_2)_{0.5}Co_3(H_2O)(OH)(PO_4)(HPO_4)(3+x)H_2O$ [29]. Co^{2+} ions are isolated in the structure, with a minimum distance Co-Co of 6.2959(2) Å. The P–O bonds exhibit a mean value of 1.5242 Å for three non-hydroxyl oxygen atoms and a slightly longer bond 1.5924(11) Å for the hydroxyl.

An alternative description of the crystal packing consists in understanding the crystal structure as inorganic layers stacked onto parallel shape to (100) plane, with the protonated molecules of piperazine inserted into these layers through N–H···O and C–H···O hydrogen bonding interactions, leading thus to the formation of an extended supramolecular network, belong to class I hybrid compounds (Table 4, Fig. 3).

Within the crystal structure of 1, there are three different hydrogen-bonding interactions. The transition metal cation interacts with hydrogenphosphate anions through

O2*w*—H1*o*2*w*···O4^{vii} and O3*w*—H2*o*3*w*···O2^{vii} hydrogen bonds (Table 4), which results in a cyclic homosynthon (8) hydrogen-bonding motif [30]. Furthermore, the $[H_2pip]^{2+}$ cation is bonded to a second hydrogenphosphate anion through the interactions N1—H1*n*1···O4^{vii} [2.210(13) Å] and N1—H1*n*1···O3^{vii} [2.283(16) Å] (Table 4), which result in a heterosynthon (5) motif (Fig. 5). Moreover, the crystal packing of 1 is also maintained by the strongest O—H···O [O3—H1*o*3···O2 = 2.7428(13) Å hydrogen bond in the stacking connecting anions, leading to an infinite chain of the formula described by the (4) graph set along the *b*-axis. In addition, the combination between these three entities, by means of intermolecular interactions, also produces three different graph-set motifs denoted as (13), (10) and (8) (Fig. 3).

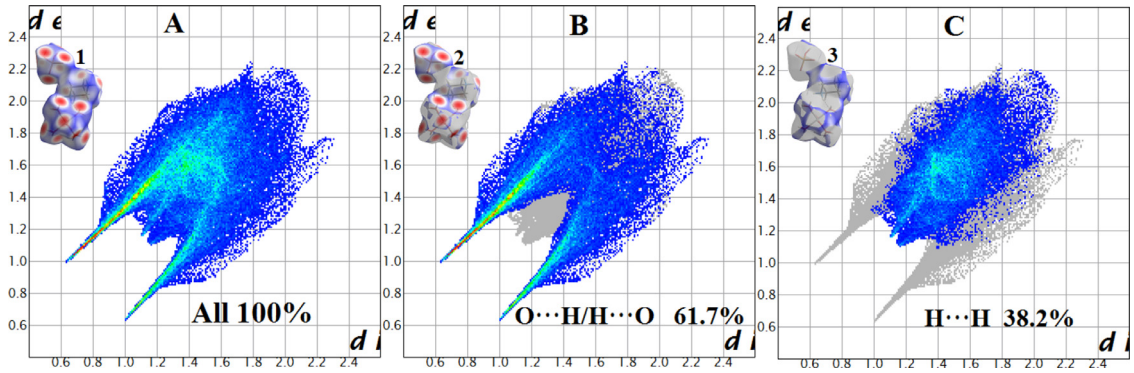

Fig. 6. 2D fingerprint plots of the HS around the asymmetric unit; the areas of the only two O···H/H···O (B) and H···H (C) intermolecular contact present are clearly shown. A, B and C surfaces to the top left highlight the relevant surface patches associated.

3.2. X-ray powder diffraction

In order to check the phase purity of the title compound, we recorded a powder XRD pattern of the grounded crystals of the title compound and compared with simulated diffraction pattern based on single crystal XRD data (Fig. 4). The measured and calculated peak positions are in good agreement, indicating phase purity, while the high intensity and sharp peaks revealed good crystallinity. So, the powder sample of the material was suitable for the further studies.

3.3. Intermolecular interactions analysis

The Hirshfeld surfaces of $(C_4H_{12}N_2)[Co(H_2O)_6](HPO_4)_2$ (Fig. 5), were analyzed to clarify the nature of the intermolecular interactions and to gain a better understanding of the three-dimensional crystal packing of 1. The visualization of the Hirshfeld three-dimensional surfaces of 1 is illustrated in Fig. 5 showing the surfaces mapped over d_{norm}. For visibility of the molecular moieties of the compound, transparent surfaces have been illustrated in a similar orientation. Each molecule in the asymmetric unit of the given crystal structure has a unique Hirshfeld surface. The information regarding intermolecular contacts presented in Table 4, is summarized effectively in the spots of the Hirshfeld surfaces mapped over d_e and d_{norm} (Fig. 5).

The hydrogen bonding contacts are visible on the d_{norm} (Fig. 5) surface with a large red circular depression, whereas the other visible spots are due to C—H···O and H···H contacts. The surfaces display several strong O···H/H···O interactions as red spots which are visible on the front and back views in the d_{norm} surfaces of the analysed compound (Fig. 5). These red spots indicate the role of the O—H···O and N—H···O hydrogen bonds for the control of crystal packing (the colour intensity indicate the relative strength of the interactions).

In the fingerprint of 1 (Fig. 6) we observe the presence of the shortest O···H/H···O contacts in the packing at ca 1.63 Å corresponding to the anion-anion O3—H1o3···O2 interactions, results in the occurrence of two long sharp spikes with a considerable contribution of H···O and O···H contacts corresponding to 61.7% of the total HS areas (Fig. 6B). In addition, the presence of these spikes at short intermolecular distances is characteristic of strong O—H ···O and N— H···O hydrogen bonds (Table 4). The molecular interactions of H···H contacts (Fig. 6C) is reflected in the middle of the scattered points in the fingerprint plots, which spread up to $(d_e + di) = 2.226$ Å and comprise 38.2% of the total HS area. They were found to be the second and the last highest contributors towards the Hirshfeld surface.

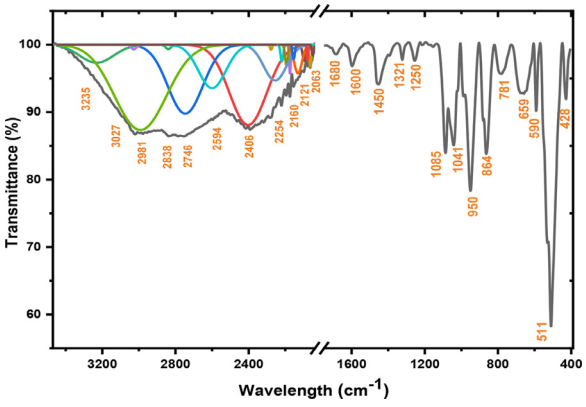

Fig. 7. FTIR spectrum of $(C_4H_{12}N_2)[Co(H_2O)_6](HPO_4)_2$.

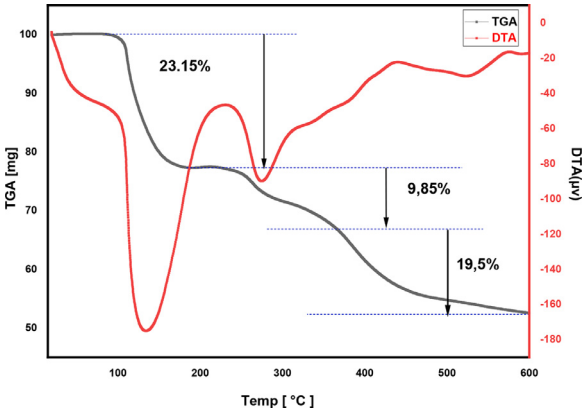

Fig. 8. TG-DTA curve for the decomposition of $(C_4H_{12}N_2)[Co(H_2O)_6](HPO_4)_2$ in air (20°C/min).

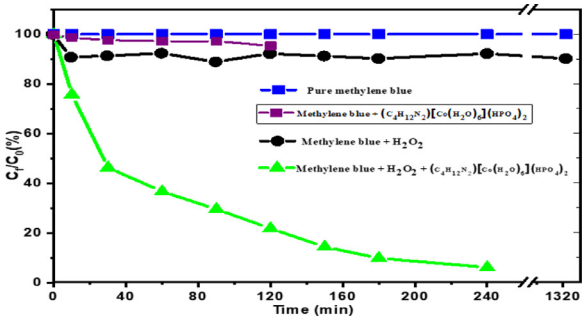

Fig. 9. The change of methylene blue concentration as a function of time after adding the hybrid cobalt phosphate.

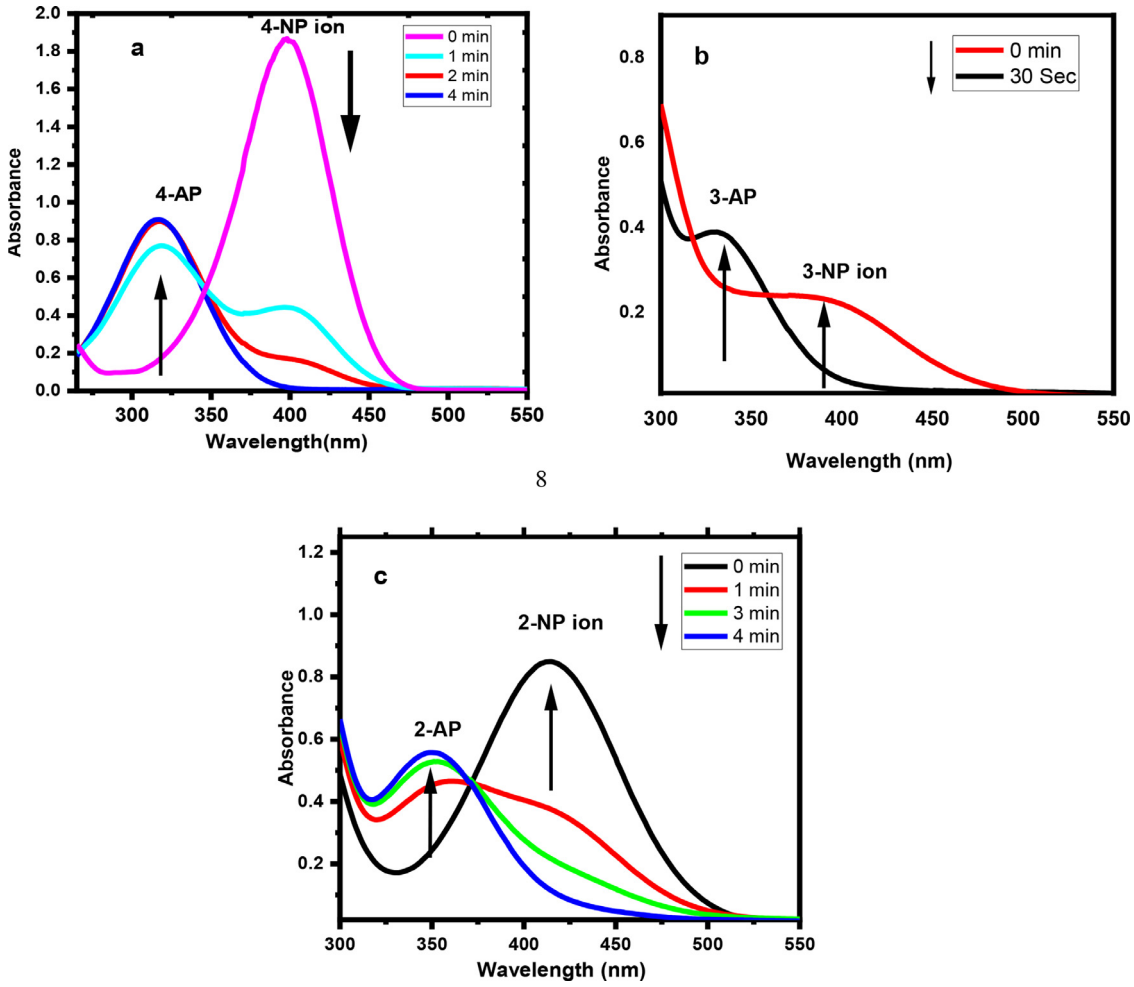

Fig. 10. Successive UV-vis spectra of the reduction of (a) 4-nitrophenol solution (4×10^{-4} M); (b) 3-nitrophenol solution (4×10^{-4} M); (c) 2-nitrophenol solution (4×10^{-4} M) in the presence of 8×10^{-4} M $NaBH_4$ using 1 as catalyst (0.1 g).

3.4. Infrared spectroscopy

Vibrational properties of complex 1 were studied with Fourier transform infrared spectroscopy (FTIR). The infrared spectrum recorded at room temperature is depicted in (Fig. 7). The set of bands appearing at 1085-659 cm^{-1} region can be attributed to the stretching modes of (HPO_4) groups. The absorbance frequency pointed at 1321 cm^{-1} is assigned to the bending vibration of the (P-OH) bonds. The asymmetric ν_{as}(P=O) stretching resonates between 1085 and 590 cm^{-1}, while the symmetric ν_s(P=O) stretch is located at 781 cm^{-1}. The absorption band observed near to 511 cm^{-1} corresponds to the asymmetric deformation of (O=P=O) bond [31]. The characteristic vibration, appearing as a medium band at 3235 cm^{-1}, boils down to the asymmetric stretching of (NH) in $(H_2pip)^{2+}$ piperazine cation. The asymmetric bending vibration of (NH_2) group is detected at 1450 cm^{-1} [32]. The broad and medium intensity band with a value of 2746 cm^{-1} belongs to the stretching vibration of (CH_2) bond [33]. The medium bands observed at around 1600 and 1680 cm^{-1} are associated to the deformation of (OH) group from water molecules while its stretching modes ν(O-H) can be related to the large absorption centered at 3027 cm^{-1} [34,35]. The medium frequencies pointing at 2838 and 2594 cm^{-1} are ascribed to the stretching vibrations of (C–C) bands, whereas the deformation modes of (C–H) groups appear as a small band at 659 cm^{-1} [36].

3.5. Thermal behavior

The thermal behaviour of the synthesised compound is shown in Fig. 8. The experimental data, given from TG analysis, shows three separated steps of weight loss in a total of 47.92% for 1. The first weight loss of 23.15%, starting at room temperature and ending at 170°C, corresponds to the removal of six water molecules accompanied by an intense endothermic signal in DTA trace at 135°C. The sharp peak indicates a vigorous and continuous weight loss (calculated: 24.15%), can be attributed to the dehydration of the cobalt compound, giving rise to the anhydrous phase $(C_4H_{12}N_2)Co(HPO_4)_2$. The second weight loss (calculated: 9.85%), observed between 200 and 350°C, is attributed to the decomposition of the half organic amine. This phenomenon is manifested with a medium endothermic peak at 275°C. The next and final step in the range of 350-560°C (Calculated weight loss 23.7%) corresponds to the decomposition of the rest of the organic molecule followed by the loss of a water molecule formed by the condensation of HO–P groups into cobalt phosphate compound. This phenomenon is coupled with a small exothermic curve.

3.6. Oxidation of methylene blue

The oxidation reaction of methylene blue dye in the presence of hydrogen peroxide (H_2O_2) was used to evaluate the catalytic

activity of the synthesized hybrid cobalt phosphate under ambient conditions. In fact, 5 mL of H_2O_2 (30%) was added to 45 mL of 6 ppm MB, and the mixture was stirred at 22°C. The variation of the concentration of MB during the reaction progress was followed at 664 nm by measuring the MB absorbance using a UV-visible spectrophotometer. As plotted in Fig. 9, and after 240 min, the concentration of pure MB has not changed, while the oxidation of MB by H_2O_2 without catalyst shows a small advancement of about 5% in the first contact and stay unchanged during the time [22,37], whilst the concentration result of mixing only pure MB and the hybrid phosphate compound seems to be inactive, with a low percentage of about 0.12%. However, by adding 0.1g of the hybrid phosphate, the concentration of methylene blue decreased until 53.84% only after 30 min, and continue decreasing till 79.46% after 120 min, to a final decrease of about 94% after 4h approximately. This result showed a very good oxidation of MB by hydrogen peroxide (H_2O_2), and confirms the catalytic efficiency of the hybrid material.

3.7. Reduction test of nitrophenol isomers

Sodium tetrahydroborate $NaBH_4$ has been widely used as an effective reducing reagent in a large number of the chemical processes, such as catalytic reduction of alcohols to hydrocarbons and selective reduction of aldehydes to alcohols [38,39]. However, borohydride does not generally reduce aromatic nitro compounds to the corresponding aniline derivatives in the absence of a catalyst [40]. In this paper, the synthesized hybrid cobalt phosphate was tested for catalytic efficiency in the reduction reaction of three nitrophenol isomers 4-NP, 3-NP, and 2-NP, using $NaBH_4$. As illustrated in Fig. 11, upon the addition of $NaBH_4$, the 4-nitrophenol was converted to the 4-nitrophenolate ion [41], and the yellow color of the solution becomes more intense. In the absence of the catalyst, the intensity of the peak at 401 nm, as well as the color of the solution, remains unchanged for several hours. However, after the addition of the catalyst, the solution becomes uncolored and the percentage of conversion of 4-nitrophenol to 4-aminophenol was observed after 1 min with the decrease in the intensity of absorption peak at 401 nm and after 4 min the peak was completely disappeared (Fig. 11a). Similarly, 3-NP and 2-NP exhibit absorption peaks at 393 nm and 415 nm, respectively, in the alkaline medium due to the formation of their corresponding nitrophenolate ions, both of which decreased readily on the addition of hybrid phosphate cobalt in company with the appearance of new peaks at 328 and 347 nm due to the formation of 3-AP and 2-AP, respectively (Fig. 10). An instantaneous reduction happened in the case of 3-NP (Fig. 10b). In contrast, the reduction reaction was slower in the case of 2-NP and 4-NP (4 min). This efficiency difference is probably due to a higher basic character of 3-NP, where the mesomeric conjugation is more important. This result illustrates the high catalytic efficiency of the prepared hybrid cobalt phosphate material in the reduction of the nitrophenol isomers compared to previous research works found in the literature [42,43].

4. Conclusion

A new hybrid phosphate, $(C_4H_{12}N_2)[Co(H_2O)_6](HPO_4)_2$, was synthesised under wet chemistry conditions and characterized by X-ray diffraction, IR-spectrometry and TG/TDA analyses. Its crystal structure consists of isolated $[Co(H_2O)_6]$ and $[PO_3(OH)]$ units linked by an extensive hydrogen-bonding network, hosting an 8-member ring of piperazine in its cavities. The intramolecular hydrogen bonds network forms different cyclic graph set motifs leading to a supramolecular assembly of anionic and cationic entities. The important role of the hydrogen bonding in the crystal cohesion was quantified by the Hirshfeld surface analysis associated with the 2-D fingerprint plots showing the prominent role of N–H··· and O–H···O interactions. Inorganic and organic moieties were confirmed by infrared spectroscopy. The hybrid compound shows promising catalytic activity in the reduction of nitro functional group in an amino group and in the oxidation and decomposition of the methylene blue dye with hydrogen peroxide under ambient conditions.

Authors contributions statement

S. Hidaoui synthesized the complex in the framework of his thesis investigation under the supervision of Prof M. Lachka, she wrote the first draft of the manuscript, in collaboration with N. Hamdi and M. Akouibaa. R. Benali-Cherif wrote the Hirshfeld part. E. Vaclav and M. Dusek solved the crystal structure and contributed to the description of the crystal structure with Brahim El Bali who led the submitted manuscript to its final version.

Declaration of Competing Interest

The authors declare that they have no known competing financial interests or personal relationships that could have appeared to influence the work reported in this paper.

References

[1] A.K. Cheetham, G. Férey, T. Loiseau, Angew. Chem. Int. Ed 38 (1999) 3268–3292.
[2] Y.U. Jihong, X.U. Ruren, Acc. Chem. Res. 43 (2010) 1195–1204.
[3] J. Wu, Y. Yan, B. Liu, X. Wang, J. Li, J. Yu, Chem. Comm. 49 (2013) 4995–4997.
[4] Y. Li, J.H. Yu, R.R. Xu, C. Baerlocher, L.B. McCusker, Angew. Chem. Int. Ed. 47 (2008) 4401–4405.
[5] Y. Wang, J.H. Yu, M. Guo, R.R. Xu, Angew. Chem. Int. Ed. 42 (2003) 4089–4092.
[6] D.F. Weng, Z.M. Wang, S. Gao, Chem. Soc. Rev. 40 (2011) 3156–3181.
[7] A. Choudhury, S. Natarajan, C.N.R. Rao, Chem. Mater. 11 (1999) 2316–2318.
[8] F. Marco, N. Lionel, R.H. Eduardo, S. Clément, Adv. Funct. Mater. 28 (2018) 1704158.
[9] S. Neeraj, M.L. Noy, C.N.R. Rao, A.K. Cheetham, J. Solid State Chem. 167 (2002) 344–353.
[10] M. Fujita, Y.J. Kwon, S. Washizu, K. Ogura, J. Am. Chem. Soc. 116 (1994) 1151–1152.
[11] R.W. Gable, B.F. Hoskins, R. Robson, J. Chem. Soc., Chem. Commun. 23 (1990) 1677–1678.
[12] C. Sassoye, T. Loiseau, F. Taulelle, G. Férey, Chem. Commun. 11 (2000) 943–944.
[13] S. Mandal, S. Natarajan, Inorg. Chem. 47 (2008) 5304–5313.
[14] L. Hu, J. Fan, C. Slebodnick, B.E. Hanson, Inorg. Chem 45 (2006) 7681–7688.
[15] AgilentCrysAlis PRO. Agilent Technologies, Yarnton, England, 2010.
[16] L. Palatinus, G. Chapuis, Superflip, J. Appl. Cryst. 40 (2007) 786–790.
[17] V. Petříček, M. Dušek, L. Palatinus, Z. Kristallogr. 229 (2014) 345–352.
[18] K. Brandenburg, H. Putz, Crystal Impact GbR, Postfach 1251, D 53002 Bonn, Germany, 2005.
[19] M.A. Spackman, J.J. McKinnon, CrystEngComm 4 (2002) 378–392.
[20] M.A. Spackman, D. Jayatilaka, CrystEngComm. 11 (2009) 19–32.
[21] S.K. Wolff, D.J. Grimwood, J.J. McKinnon, M.J. Turner, D. Jayatilaka, M.A. Spackman, Crystal Explorer, Version 3.1 (2012).
[22] N. Hamdi, S. Hidaoui, H.O. Hassani, M. Lachkar, M. Dusek, N. Morley, B. El Bali, J. Mol. Struct. 1217 (2020) 128317.
[23] N.L. Nkhili, W. Rekik, H. Naïli, T. Mhiri, T. Bataille, Solid State Phenom 194 (2013) 171–174.
[24] J.X. Pan, G.Y. Yang, Y.Q. Sun, Acta Crystallographica Section E: Structure Reports Online 59 (2003) m286–m288.
[25] K. Robinson, G.V. Gibbs, P.H. Ribbe, Science 172 (1971) 567–570.
[26] M.E. Fleet, Mineral. Mag. 40 (1976) 531–533.
[27] F.A.I. Ngopoh, M. Lachkar, T. Đordević, C.L. Lengauer, B. El Bali, J. Chem. Crystallogr. 45 (2015) 369–375.
[28] R. Ouarsal, B. El Bali, M. Lachkar, M. Dusek, K. Fejfarova, Acta Cryst E61 (2005) i168–i170.
[29] W.K. Chang, R.K. Chiang, S.L. Wang, J. Solid State Chem. 180 (2007) 1713–1719.
[30] J. Bernstein, R.E. Davis, L. Shimoni, N.L. Chang, Angew. Chem. Int. Ed. 34 (1995) 1555–1573.
[31] N. Bouzidia, N. Salah, B. Hamdi, A. Ben Salah, J. Mol. Struct 1134 (2017) 797–805.
[32] C.R. Saha, J. Inorg, Nucl. Chem. 38 (1976) 1635–1640.
[33] N. Prabavathi, A. Nilufer, V. Krishnakumar, Spectrochim, Acta Part A: Molecular and Biomolecular Spectroscopy 121 (2014) 483–493.
[34] A. Novak, Hydrogen bonding in solids correlation of spectroscopic and crystallographic data, Large Molecules. Structure and Bonding, Springer, Berlin/Heidelberg, Germany, 1974, pp. 177–216.
[35] G. Gilli, P. Gilli, J. Mol. Struct. 552 (2000) 1–15.

[36] X. Zhang, G.M. Wang, Z.H. Wang, Y.X. Wang, J.H. Lin, J. Mol. Struct. 1056-1057 (2014) 25–30.
[37] H.O. Hassani, M. Akouibaa, S. Rakass, M. Abboudi, B. El Bali, M. Lachkar, F. Al Wadaani, Journal of Science: Advanced Materials and Device (2022) doi.org/10.1016/j.jsamd.2021.06.003.
[38] G.W. Gribble, Chem. Soc. Rev. 27 (1998) 395–404.
[39] M. Periasamy, P. Thirumalaikumar, J. Organomet. Chem. 609 (2000) 137–151.
[40] G.W. Kabalka, R.S. Varma, Reduction of Nitro and Nitroso Compounds, In Comprehensive Organic Synthesis, Elsevier, Pergamon, 1991, pp. 363–379.
[41] Z. Jin, M. Xiao, Z. Bao, P. Wang, J. Wang, Angew. Chem. Int. Ed. 51 (2012) 6406–6410.
[42] H.O. Hassani, S. Rakass, M. Abboudi, A. Mohmoud, F. Wadaani, Molecules 23 (2018) 1462.
[43] H.O. Hassani, Catal. Commun. 60 (2015) 19–22.